Published in final edited form as:
J Immunol. 2009 February 15; 182(4): 2277–2287. doi:10.4049/jimmunol.0802775.

Immune Reconstitution during *Pneumocystis* Lung Infection: Disruption of Surfactant Component Expression and Function by *S*-Nitrosylation[1]

Elena N. Atochina-Vasserman[2,*], **Andrew J. Gow**[†], **Helen Abramova**[*], **Chang-Jiang Guo**[†], **Yaniv Tomer**[*], **Angela M. Preston**[‡], **James M. Beck**[‡], and **Michael F. Beers**[2,*]

[*]Division of Pulmonary, Allergy, and Critical Care Medicine, Department of Medicine, University of Pennsylvania School of Medicine, Philadelphia, PA 19104

[†]Department of Pharmacology and Toxicology, Ernest Mario School of Pharmacy, Rutgers University, Piscataway, NJ 08854

[‡]Division of Pulmonary and Critical Care Medicine, Department of Internal Medicine, University of Michigan Medical School, and Veterans Affairs Medical Center, Ann Arbor, MI 48109

Abstract

Pneumocystis pneumonia (PCP), the most common opportunistic pulmonary infection associated with HIV infection, is marked by impaired gas exchange and significant hypoxemia. Immune reconstitution disease (IRD) represents a syndrome of paradoxical respiratory failure in patients with active or recently treated PCP subjected to immune reconstitution. To model IRD, C57BL/6 mice were selectively depleted of $CD4^+$ T cells using mAb GK1.5. Following inoculation with *Pneumocystis murina* cysts, infection was allowed to progress for 2 wk, GK1.5 was withdrawn, and mice were followed for another 2 or 4 wk. Flow cytometry of spleen cells demonstrated recovery of $CD4^+$ cells to >65% of nondepleted controls. Lung tissue and bronchoalveolar lavage fluid harvested from IRD mice were analyzed in tandem with samples from CD4-depleted mice that manifested progressive PCP for 6 wks. Despite significantly decreased pathogen burdens, IRD mice had persistent parenchymal lung inflammation, increased bronchoalveolar lavage fluid cellularity, markedly impaired surfactant biophysical function, and decreased amounts of surfactant phospholipid and surfactant protein (SP)-B. Paradoxically, IRD mice also had substantial increases in the lung collectin SP-D, including significant amounts of an *S*-nitrosylated form. By native PAGE, formation of *S*-nitrosylated SP-D in vivo resulted in disruption of SP-D multimers. Bronchoalveolar lavage fluid from IRD mice selectively enhanced macrophage chemotaxis in vitro, an effect that was blocked by ascorbate treatment. We conclude that while PCP impairs pulmonary function and produces abnormalities in surfactant components and biophysics, these responses are exacerbated by IRD. This worsening of pulmonary inflammation,

[1]This work was supported by National Institutes of Health Grants R01 HL64520 (to M.F.B.) and R01 HL083482 (to J.M.B.).

[2]Address correspondence and reprint requests to: Dr. Michael F. Beers and Dr. Elena N. Atochina-Vasserman, Pulmonary and Critical Care Division, University of Pennsylvania School of Medicine, H410F Hill Pavilion, 380 S. University Avenue, Philadelphia, PA 19104. mfbeers@mail.med.upenn.edu and atochina@mail.med.upenn.edu.

Disclosures
The authors have no financial conflicts of interest.

in response to persistent *Pneumocystis* Ags, is mediated by recruitment of effector cells modulated by *S*-nitrosylated SP-D.

Pneumocystis pneumonia (PCP)[3] has long been recognized as an opportunistic infection affecting immunocompromised patients (1–4). Host defense factors are considered important determinants of susceptibility to the pathogen. Diseases affecting cell-mediated immunity, such as leukemia, SCID, and HIV infection, are classically associated with PCP, but the infection has been reported as a complication of a wide range of other immunosuppressive conditions (reviewed in Refs. 4, 5). Respiratory failure continues to represent a major sequel of PCP. While alveolar infiltrates appear on the chest radiograph, the degree of hypoxemia, altered lung mechanics, and increased work of breathing are often out of proportion to the severity of the radiographic findings, suggesting the existence of intrapulmonary shunting and microatelectasis. Work from this laboratory and others has provided evidence that PCP, both directly and via the host inflammatory response, induces dysfunction of the pulmonary surfactant system (6–12).

Pulmonary surfactant is a surface-active mixture of phospholipid and protein secreted by alveolar type II cells that reduces surface tension at the air-liquid interface, permitting alveolar stability throughout the respiratory cycle (12, 13). In addition to lipid, biochemical analyses have characterized four unique surfactant-associated proteins (SP) designated SP-A, SP-B, SP-C, and SP-D (reviewed in Refs. 14, 15), which can be subdivided into two groups based on structure, function, and solubility. The hydrophobic proteins SP-B and SP-C are involved in adsorption of lipid at the air-liquid interface (16, 17). The more hydrophilic proteins, SP-A and SP-D, do not contain significant intrinsic biophysical activity but are members of a growing family of proteins that plays a role in the innate or non-Ab-mediated immune response (18). The term collectin (collagen-like lectin) has been used to describe this family whose non-lung members include serum proteins man-nose-binding lectin, bovine conglutinin, and CL-43 (19). SP-A and SP-D are recognized as important components of the pulmonary innate immune system modulating complex interactions that occur between pathogens and host effector cells (reviewed in Ref. 20).

SP-D is a single gene product that can be detected both in type II cells and Clara cells (21, 22). Monomeric SP-D (43 kDa) contains a collagen-like triple helical domain and a calcium-dependent carbohydrate recognition domain (21). Biosynthesis of SP-D includes assembly of monomeric SP-D into trimers followed by oligomerization of four trimers via critical cysteine residues at positions 15 and 20 located within the hydrophobic tails to produce a dodecamer (23, 24). When fully assembled, SP-D is capable of mediating a variety of functions, including aggregation of pathogens, lysis of microbes, enhancement of phagocytosis, modulation of cytokines and reactive species, and mediation of effector cell proliferation.

[3]Abbreviations used in this paper: PCP, *Pneumocystis* pneumonia; SNO, *S*-nitrosothiol; BALF, bronchoalveolar lavage fluid; iNOS, inducible nitric oxide synthase; IRD, immune reconstitution disease; LA, large aggregate; SA, small aggregate; SP-A, pulmonary surfactant protein A (35 kDa); SP-B, pulmonary surfactant protein B (9 kDa); SP-C, pulmonary surfactant protein C (3.7 kDa); SP-D, pulmonary surfactant protein D (43 kDa).

The mechanistic regulation of the observed pro- and antiinflammatory functions of SP-D is incompletely defined. However, based on data published for SP-A, which has a similar functional duality, it has been suggested that proinflammatory functions of collectins are mediated by tail domains, via binding to CD91 and calreticulin, and antiinflammatory functions by the head domains, via binding to signal regulatory protein-α (SIRPα). Recent work from our group has shown that both in vitro and in vivo, SP-D is capable of undergoing posttranslational modification by NO to produce *S*-nitrosylated forms that disrupt higher order oligomerization. Furthermore, *S*-nitrosylated SP-D (SNO-SP-D) serves as a proinflammatory mediator enhancing macrophage migration and lung chemokine production (25).

Immune reconstitution disease (IRD) in response to a number of microorganisms has been described in patients immunosuppressed by HIV infection and by other mechanisms, including chemotherapy (26–30). In the context of PCP, this syndrome encompasses an acute symptomatic respiratory decompensation that is related temporally to treatment of PCP coupled with reconstitution of host immune processes (such as reduction in the dosage of corticosteroids and/or cytotoxic agents or a reduction in HIV viral load). This combination results in the development of immunopathologic lung damage and acute respiratory failure. Although highly active antiretroviral therapy has led to a decrease in opportunistic infections (31), paradoxical worsening of lung function and respiratory failure have been reported after the beginning of highly active antiretroviral therapy in patients treated for PCP (26–30). It has been proposed that this phenomenon results from transient worsening of inflammation due to pulmonary recruitment and activation of immune cells responding to persistent *Pneumocystis* cysts or Ags.

Immmune reconstitution in the setting of PCP has been predominantly modeled in murine hosts using selective transfer of lymphocyte subsets. *Pneumocystis murina*-infected *scid* mice subjected to direct immunologic reconstitution with selective populations of sensitized CD4 and/or CD8 T cells mount protective responses to the organism that results in focal areas of pulmonary inflammation marked by elaboration of IL-1β, IL-6, IFN-γ, as well as macrophage-derived TNF-α near the sites of cell-organism contact (9, 32–36). In the present study we have modified an established and validated model of PCP that utilizes selective depletion of $CD4^+$ cells from mice followed by intratracheal inoculation with *P. murina* (37–39). To model IRD, withdrawal of the depleting Ab was performed before the development of overt PCP (~2 wk). We found that during the ensuing 4 wk, these reconstitutions produce significant pulmonary inflammatory responses characterized by depletion and dysfunction of hydrophobic pulmonary surfactant components. Additionally, selective up-regulation of SP-D expression occurs accompanied by alterations in its quaternary structure and function mediated by local *S*-nitrosylation of SP-D monomers. These findings represent a novel paradigm for modulation of lung inflammation by an intrinsic innate host defense protein subjected to a selective, nonenzymatic posttranslational modification. Furthermore, the results also extend our understanding of the mechanisms of IRD during PCP that could suggest novel therapeutic approaches for this increasingly important clinical problem.

Materials and Methods

Antisera

Monospecific, polyclonal surfactant protein antiserum against SP-B has been previously characterized in detail (40). A monospecific, polyclonal Ab against SP-D (AB 1754) was produced in rabbits using synthetic peptides corresponding to two homologous regions of the mouse/human SP-D sequences as the immunizing Ag and has been previously described (41). This Ab recognizes denatured isoforms of mouse SP-D as well as both denatured and native forms of human SP-D. A polyclonal antiserum against recombinant mouse SP-D was purchased from Chemicon. This antiserum recognizes multiple isoforms (native greater than denatured) of murine SP-D.

Mouse model of *Pneumocystis* infection and immunoreconstitution

C57BL/6 mice were purchased from Charles River Laboratories and housed in a barrier isolation animal care facility at the University of Pennsylvania in filter-top cages for 7 days before inoculation. Experiments were performed between 8 and 14 wk of age on male and female mice. Mice received sterile rodent chow and sterile drinking water. Normal sentinel mice were examined routinely for the presence of unintended pathogens by culture and serology. The Institutional Animal Care and Use Committees of the University of Pennsylvania reviewed and approved all animal procedures.

Organisms—*P. murina* organisms were obtained from the lungs of athymic mice (*nu*/*nu* on a BALB/c background from Taconic Laboratories) in which *Pneumocystis* organisms are propagated by serial passage as previously described (37). Before dispersal of *P. murina* by homogenization using a Stomacher apparatus, bacterial contamination was excluded by the routine use of Gram staining of touch preparations of each harvested lung. Following centrifugation, organisms collected in the resulting pellet were stained with modified Giemsa stain, counted, and then inoculated intratracheally (0.1 ml = 2×10^5 *P. murina* cysts) into anesthetized mice.

Generation of *P. murina* infection and IRD—The experimental design utilized in these studies is illustrated in Fig. 1. C57BL/6 mice were subjected to selective CD4 depletion via i.p. injection twice weekly with the mAb GK1.5 as previously published (42–44). Control mice received i.p. injection of equal volumes of PBS. One week after initiation of CD4 depletion, experimental animals were intratracheally inoculated under direct visualization with 2×10^5 *P. murina* cysts harvested from the colony of *P. murina*-infected *nu*/*nu* mice. Following inoculation, *P. murina* infection was allowed to progress for 2 wk before initiation of immune reconstitution through withdrawal of GK1.5 Ab for an additional 2 or 4 wk as indicated (i.e., IRD). As positive controls, mice inoculated with *P. murina* were subjected to continuous CD4 depletion with GK1.5 for up to 6 wk.

FACS analysis of CD4 cells—Flow cytometric analysis was used to verify depletion of $CD4^+$ T cells at the time of inoculation and to track immune reconstitution after withdrawal of GK1.5 treatment. At indicated time points, spleens from nondepleted, depleted, and immune-reconstituted mice were passed through a wire mesh, and splenocytes were isolated

by gradient centrifugation with Histopaq-1077 (Sigma-Aldrich). Cells (5×10^5/well) were incubated on ice for 30 min with FITC-labeled anti-CD3 and allophycocyanin-labeled anti-CD4 (clone RM4-5) or isotype-matched irrelevant Abs (all from BD Pharmingen). Data were collected on a FACSCalibur flow cytometer and analyses were performed using CellQuest software (BD Biosciences). Data are expressed as a percentage of CD3 cells with positive staining for CD4.

Quantitation of pneumocystis infection—The magnitude of viable organism burden in *P. murina*-inoculated mice was assessed by quantitative RT-PCR using the method of Zheng et al. (45). Total RNA was isolated from the left lungs of infected mice by a single-step method using TRIzol reagent (Invitrogen). Plasmids containing *P. murina* rRNA (a kind gift from Dr. Chad Steele, University of Alabama-Birmingham) were used as a standard for the assay. The template was digested with RNase-free DNase, quantitated by spectrophotometry, and aliquoted at −80°C until further use. The Taq-Man PCR primers for mouse *Pneumocystis* rRNA are 5′-ATG AGG TGA AAA GTC GAA AGG G-3′ and 5′-TGA TTG TCT CAG ATG AAA AAC CTC TT-3′. The probe was labeled with a reporter fluorescent dye, FAM, and the sequence was FAM-AAC AGC CCA GAA TAA TGA ATA AAG TTC CTC AAT TGT TAC-TAMRA. Real-time PCR was conducted using one-step TaqMan RT-PCR reagents (Applied Biosystems). The PCR amplification was performed for 40 cycles, with each cycle at 94°C for 20 s and 60°C for 1 min, in triplicate using the ABI Prism 7700 SDS. Threshold cycle values were averaged triplicate reactions, and data were converted to rRNA copy number by using a standard curve of known copy number of *P. murina* rRNA. This assay has a correlation coefficient >0.98 over 8 logs of *P. murina* rRNA concentration and correlates with viable organism counts.

Lung tissue

Histology and inflammation scores—Following lavage, left lungs were removed and frozen in liquid nitrogen for RT-PCR analysis; right lungs were inflated and fixed with paraformaldehyde (4% in 0.1 M sodium cacodylate (pH 7.3)) for histological analysis. Paraffin-embedded lung sections stained with H&E were used to evaluate the intensity of pulmonary inflammation. Sections were scored in a blinded fashion by two independent observers to grade the intensity of inflammation using a previously validated scoring system (42).

RT-PCR for CD4/CD8 expression—To determine the microenvironment of the lung parenchyma subjected to IRD, CD4 and CD8 mRNA levels in harvested lung tissue were quantitated by RT-PCR as described by Phares et al. (46) and Jassare et al. (47). Total RNA used for determination of *P. murina* rRNA described above was reverse transcribed using the TaqMan reverse transcription reagents kit (Applied Biosystems). CD4 and CD8 were then amplified using the following primers: CD4 (3′-GAG ATT ATG GCT CTT CTG CAT, 5′-ATC AGG AAG TGA ACC TGG TG) and CD8 (3′-TTC TCT GAA GGT CTG GGC TT, 5′-CAG CAA CTC GGT GAT GTA CT), a kind gift from Dr. Steven Albelda (University of Pennsylvania). PCR amplification of triplicate cDNA was performed on an Applied Biosystems 7500 Fast real-time PCR system for 40 cycles, with each cycle at 95°C for 15 s and 60°C for 1 min. Ct values obtained using Sequence Detection Software version

1.4 (Applied Biosystems) were determined, and relative amounts of specific mRNA were calculated using the relative quantitation (ΔΔCt) method and expressed as fold change. 18S RNA served as the endogenous control (assayed using a TaqMan gene expression assay from Applied Biosystems).

Bronchoalveolar lavage fluid (BALF) analyses

Cell counts—Lungs were lavaged with 0.5-ml aliquots of sterile saline to a total of 5 ml. Recovered BALF samples were centrifuged (400 × *g* for 10 min) and the cell pellet was gently resuspended in 1 ml of PBS (with Ca^{2+} and Mg^{2+}) for total cell count determination using a Z1 Counter particle counter (Beckman Coulter). Aliquots of cells were spun on a Thermo Shandon Cytospin-3 at 750 rpm for 3 min and stained with standard Diff-Quik for manual determination of cell differentials. Cells were identified as macrophages, eosinophils, neutrophils, and lymphocytes by standard morphology.

Analysis of surfactant components—Cell-free BALF supernatants were separated into large-aggregate (LA) and small-aggregate (SA) fractions by centrifugation (20,000 × *g* for 60 min at 4°C) as described previously (7). Total protein content of LA and SA fractions was determined by the method of Bradford, with bovine IgG as a standard (48). Total phospholipid content of LA and SA fractions was determined by the method of Bartlett (49).

Surface tension measurements—The biophysical activity of recovered surfactant from all experimental groups was measured in a capillary surfactometer (Calmia Medical) as described in detail previously (7, 50, 51). Briefly, LA fractions of BALF were diluted with saline to a total phospholipid concentration of 1 mg/ml and 0.5-μl samples and then introduced into the glass capillary of the capillary surfactometer and compressed for 120 s, resulting in cyclic extrusion from the narrow end of the capillary permitting airflow during capillary patency. The percentage of the 120-s study period that the capillary is patent was calculated and data were expressed as percentage openness. Each sample was analyzed in triplicate.

PAGE and immunoblotting—BALF proteins were separated and analyzed by two methods. Denaturing SDS-PAGE was performed under reducing conditions using 10–20% Novex tricine gels for SP-B and NuPAGE Novex 10% Bis-Tris gels for SP-D (all from Invitrogen).

Native gel electrophoresis for detection of SP-D quaternary structure was performed using NuPAGE 3–8% Tris-acetate (Invitrogen) as previously described (25). Calculated equal amounts of SP-D determined first using SDS-PAGE as described above were mixed with a cold native Tris-glycine sample buffer before loading. Electrophoresis was run at room temperature at a constant voltage of 150 V for 2 h. Proteins were then transferred to polyvinylidene difluoride membranes.

Separated proteins (1 μg of total protein per lane) were transferred to nitrocellulose at room temperature using Tris-glycine transfer buffer at 30 V overnight. Blots were blocked for 1 h at room temperature with 10% nonfat milk and then incubated with primary SP-B (1/5000 dilutions) or SP-D Ab (1/20,000 dilution) for 1 h. The intensity of bands visualized using

HRP-conjugated goat anti-rabbit IgG (Jackson ImmunoResearch Laboratories) and ECL (Amersham Biosciences) were quantitated by densitometric scanning of exposed films or direct acquisition on a Kodak 440 imaging system.

Biotin switch assay for detection of SNO-SP-D—Detection of SNO-SP-D was performed via an adaptation of the biotin switch method (52). BALF (30 μg of total protein) was diluted in HEN buffer (25 mM HEPES (pH 7.7), 0.1 mM EDTA, 0.01 mM neocuproine) and 20 μM *N*-ethylmaleimide at 37°C for 30 min to block free thiols. Excess *N*-ethylmaleimide was removed by protein precipitation using cold acetone. Protein pellets were resuspended in diethylenetriaminepentaacetic acid and *S*-nitrosothiol (SNO) bonds decomposed by adding 20 mM sodium ascorbate. The newly formed thiols were linked with the sulfhydryl-specific biotinylating reagent *N*-[6-biotinamido)-hexyl]-1-(2-pyridyldithio)propionamide (biotin-HPDP; Pierce Biotechnology). Biotinylated proteins were precipitated with streptavidinagarose beads, and Western blot analysis was performed to detect the amount of captured SP-D using polyclonal SP-D antiserum.

NO measurements—BALF samples were analyzed for NO metabolites by chemical reduction and chemiluminescence using the Ionics/Sievers nitric oxide analyzer 280 (NOA 280; Ionics Instruments), as previously described (53). All nitrogen oxides were reduced by use of an excess of vanadium chloride in hydrochloric acid at 95°C, and measurements using these conditions were considered as a total nitrogen oxide measurement.

Nitrite was measured independently and subtracted from the total NO to calculate the concentration of nitrate. Nitrite analysis was performed using a KI and acetic acid mixture at room temperature (54). Resultant signal areas from each assay were compared with standards to calculate the concentration of each nitrogen oxide. Sodium nitrate and nitrite (Sigma-Aldrich) were utilized as the standards for the vanadium and iodide assays, respectively.

Measurement of cytokines—Sandwich ELISA assays of BALF from all groups for levels of MCP-1 (CCL2), eotaxin, and KC were performed using Quantikine kits from R&D Systems following the manufacturer's instructions. BALF IFN-γ and TNF-α were measured using sandwich ELISA kits from BD Pharmingen. All samples were assayed in duplicate.

Chemotaxis assay—Directed migration (chemotaxis) of cells was performed as previously described (25). Briefly, 50 μl of RAW 264.7 cells (American Type Culture Collection), suspended at 2×10^6 cells per ml in DMEM, was placed in the upper wells of a 48-well microchemotaxis chamber (Neuro Probe). The lower chambers contained 40 μl of test solution, consisting of DMEM and either saline (control) or BALF from PCP infected or reconstituted mice. A polyvinylpyrrolidone-free polycarbonate filter (5-μm pores) was placed between the wells along with the rubber gasket of the assembly. The chamber was incubated for 3 h at 37°C with 5% CO_2. Nonmigrating cells were scraped from the upper surface, and the filter containing migrating cells was stained with Hemacolor differential blood stain and mounted on a glass coverslip. Cells migrated through the filter were counted in 10 randomly selected oil-immersion fields in each well at ×100 magnification. Data were expressed as the average of the three fields in cells per oil-immersion field.

Statistical analysis

Data analyses were performed using GraphPad InStat v3.06 for Windows (GraphPad Software). Parametric data were analyzed with ANOVA or Student's *t* test assuming equal variances to test differences between groups. Data were expressed as mean ± SEM. Nonparametric data were analyzed by the Wilcoxon/Kruskal-Wallis rank sum test. Data were expressed as median values. In all cases a p value of <0.05 was considered as significant.

Results

Kinetics of *P. murina* infection and CD4 cell recovery in a model of IRD

Administration of two doses of GK1.5 mAb resulted in complete depletion of peripheral $CD4^+$ T cells (Fig. 2*A*). Following withdrawal of the Ab 2 wk after intratracheal inoculation of *P. murina*, CD4 T cells in the periphery recovered over the ensuing 4 wk, reaching 65% of nondepleted mouse levels.

In mice persistently depleted of CD4 cells, progressive infection with *P. murina* occurred. Using a sensitive and quantitative RT-PCR protocol, *P. murina*-specific rRNA was detected at 2 wk postinoculation and increased progressively to week 6 (Fig. 2*B*). In contrast, the *P. murina* burden in mice undergoing immune reconstitution at week 2 had similar degrees of viable organisms 4 wk after inoculation. However, following the return of significant numbers of peripheral CD4 T cells (4 wk), there was a significant reduction in *P. murina* burden in the IRD group.

Quantification of lung inflammation and cellular accumulation

Despite significantly lower organism burdens, IRD mice infected with *P. murina* developed equivalent amounts of parenchymal pulmonary inflammation (Fig. 3*A*). Scoring of histopathology from these groups demonstrated progressive cellular inflammation in the CD4-depleted group through 6 wk postinoculation, which was similar to that observed in the IRD group even 4 wk after GK1.5 withdrawal (Fig. 3*B*). Furthermore, using RT-PCR to detect expression of T cell surface Ags (Fig. 4), the lung parenchyma from the IRD group was found to be infiltrated with a combination of CD4 and CD8 cells while, as expected and consistent with previous reports (55), lung tissue from the CD4-depleted group infected with *P. murina* had marked increases in CD8 expressing cells.

The increase in parenchymal cellular infiltrates in IRD mice was accompanied by a commensurate increase in total BALF cell counts (Fig. 5*A*). Diff-Quik staining of cytospins from the BALF subjected to differential cell counting demonstrated that the alveolar cell population consisted predominantly of macrophages but also had a significant degree of neutrophilia and increased numbers of lymphocytes (Fig. 5*B*).

Measurement of lung injury and alteration in surfactant components

Importantly, despite a >95% reduction in *P. murina* organism burden, at 6 wk postinoculation (and 4 wk postreconstitution), IRD mice continued to display elevated amounts of total BALF protein similar in magnitude to persistently infected mice (Fig. 6*A*).

This finding was also reflected in increased lung-to-body weight ratios in both groups (Fig. 6*B*). Taken together, the indices of lung injury following IRD are enhanced relative to the degree of infection. These changes in cellularity and protein leak were not seen when mice were CD4 depleted, inoculated with lung homogenate from uninfected *nu*/*nu* (BALB/c background) donors, and then subjected to immune reconstitution, indicating that the inflammatory responses were not attributable to the use of allogenic donor mice (Fig. 7).

Inflammatory mediators present in the BALF of the injured groups were also assessed. Both *P. murina*-infected and IRD mice demonstrated elevations in total BALF NO and its oxidative forms (nitrates) (Fig. 6, *C* and *D*). Multiplex BALF cytokine analysis revealed that 6 wk after inoculation, there were marked elevations in MCP-1 in both *P. murina*-infected (CD4 depleted) mice as well as IRD ("2 + 4") mice, although the increases were slightly greater in the IRD group (Table I). Compared with uninfected controls, IRD mice had significant increases in KC and IFN-γ, while *P. murina*-infected (6 wk) groups had significant elevations in IFN-γ, but there were no differences between the two groups.

Biochemical analysis of BALF revealed that 6 wk postinoculation, despite the marked variations in organism burden, CD4-depleted and IRD mice each had marked decreases in SP-B levels in the biophysically active large aggregate surfactant fraction (Fig. 8*A*), which was accompanied by similar decreases in total phospholipid (Fig. 8*B*). The alterations in SP-B protein and phospholipid contents were reflected in a dysfunctional surfactant in both groups where, using a capillary surfactometer, moderate reductions in surface activity could be seen (Fig. 8*C*). Consistent with the results obtained for cell counts and BALF protein (Fig. 7), total phospholipid in large aggregate surfactant fractions was not altered in mice receiving intratracheal uninfected BALB/c lung homogenate followed by withdrawal of GK1.5 (data not shown).

IRD promotes nitrosylation of SP-D

Despite decreases in SP-B and phospholipid that evolved during immune reconstitution, SP-D levels were significantly increased in mice subjected to immune reconstitution within 2 wk after withdrawal of GK1.5. By Western blotting and quantization, IRD mice had SP-D levels that were 3-fold higher than uninfected controls and 60% greater than mice continuously infected with *P. murina* (Fig. 9*A*). Recently, we have shown that inflammatory lung injury can induce alterations in SP-D structure and function through *S*-nitrosylation of cysteine residues in its NH_2 tail region (25). We therefore subjected BALF from these mice to analysis for the presence of SNO-modified SP-D and performed native gel electrophoresis to determine molecular subspecies of SP-D. As shown in Fig. 9*B*, using a biotin derivitization method, SP-D in the BALF of immunoreconstituted mice showed increased levels of *S*-nitrosylation that were accompanied by marked alterations in quaternary structure. Under these electrophoresis conditions, native SP-D from CD4-depleted mice with *Pneumocystis* infection is too large (M_r > 800,000) to enter the 10% resolving gel and it remains in the wells (Fig. 9*C*). Similar patterns were obtained for BALF from uninfected mice (data not shown). In contrast, BALF from IRD mice that contained marked amounts of *S*-nitrosylated SP-D exhibited significant amounts of smaller molecular forms (trimers).

Taken together, these data indicate that a selective and specific modification of SP-D by NO occurs during the inflammatory response associated with IRD.

We have recently shown that *S*-nitrosylated SP-D could alter the chemotactic ability of macrophages (25). Both *P. murina* infection and IRD produced increases in alveolar macrophage numbers 6 wk after *Pneumocystis* inoculation. Based on this, we hypothesized that under conditions of IRD, the alterations in SP-D structure we observed could functionally promote macrophage chemotaxis. We examined the ability of both modified and unmodified SP-D to act as a chemoattractant for macrophages. Utilizing a modified Boyden chamber with RAW cells as the target, BALF from IRD mice promoted significantly greater chemotaxis than did that from CD4-depleted animals (Fig. 10). Pretreatment of the BALF with ascorbate, which removes the NO moiety from SNO, significantly reduced the chemotactic efficacy of BALF to levels similar to those seen with PCP and CD4 depletion.

Discussion

The coordinated regulation of the immune response to promote organism clearance and then limit local tissue damage is crucial to effective lung host defense. Multiple studies have shown that CD4 T cells are essential for proper clearance of *Pneumocystis* pulmonary infection (36, 38, 56). Clinically, several case reports and series have detailed PCP patients who have undergone immune recovery and developed acute respiratory failure (26 –29). We have developed a murine model of IRD in which the return of native $CD4^+$ T cells through the withdrawal of an immunosuppressive mAb, GK1.5, mimics the clinical disease in humans. In this model, as in humans with IRD, we observed marked increases in pulmonary inflammation and lung injury parameters despite significantly attenuated *P. murina* burden. Utilizing this model, the present study extends previous observations of IRD pathogenesis through identification of a novel form of SP-D post-translationally modified by *S*-nitrosylation that profoundly alters its normal immunosuppressive effects on lung effector cell function.

It has been previously well documented that in the pathogenesis of respiratory failure in PCP, the surfactant system plays important role in the modulation of lung mechanics and of gas exchange (7–9). In the present study, we documented changes in surfactant component expression and biophysical activity, including selective down-regulation of phospholipid and SP-B along with corresponding increases in surface tension. However, immune reconstitution resulted in an equally pronounced surfactant dysfunction, suggesting that the host response to residual *Pneumocystis* organisms or Ags can further modulate inhibition of surfactant activity. Coupled with the finding that uninfected lung homogenate failed to generate either a significant inflammatory injury (Fig. 7) or disruption of surfactant component expression, anti-*Pneumocystis* responses that occurred during CD4-mediated immune recovery were responsible for the observed enhancement of lung injury in mice and could be similarly responsible for the significant morbidity observed in patients with PCP and IRD.

While *Pneumocystis* organisms have been shown to attach directly to alveolar epithelial cells (57), it is unlikely that *Pneumocystis* is playing a direct role in the IRD-mediated lung damage. In vitro we have shown that *P. murina* does not alter alveolar epithelial cell barrier function (58), indicating that it is more likely that local inflammatory effector cells are mediating the observed lung damage. Furthermore, in the present study, equivalent or greater injury occurred despite decreased burdens of *P. murina*. The lungs of IRD mice showed increased lung edema and lung-to-body weight ratios. Previously, other investigators have utilized reconstitution with bone marrow-derived CD4 and CD8 cells to model *Pneumocystis*-induced IRD in *scid*/*scid* mice (33, 34, 36, 59). Under normal circumstances, this strain typically develops low levels of pulmonary inflammation despite high organism burdens. When reconstituted with CD4 cells, those mice developed marked increases in lung injury and gross physiological changes associated with decreased lung compliance. Although the molecular mechanisms underlying the observed findings were not completely defined, the time course (4–6 wk) for lung injury seen in those studies appears to be similar to the model utilized for the present study.

In this model, histological scores of parenchymal inflammation were significantly increased in both *P. murina*-infected and IRD groups (Fig. 3*B*). However, using more sensitive methods, we were able to detect subtle differences in the cellular composition of the inflammatory response that were consistent with immune reconstitution. By RT-PCR, the infiltration of the lung parenchyma that occurred during IRD consisted of both CD4 and CD8 expressing cells, while responses in CD4-depleted (GK1.5-treated) mice infected with *P. murina* were limited to CD8 cells (Fig. 5). Furthermore, in addition to alterations in lung parenchymal infiltration, there was a relatively greater increase in BALF cells late in the course in IRD mice compared with their *P. murina*-infected CD4-depleted counterparts (Fig. 4). The histology and accompanying scoring reflect primarily parenchymal inflammation from accumulation of inflammatory cells in the tissue. In contrast, cells recovered in the BALF reflect effector cells that have traversed into the airspaces. The observed dichotomy between parenchyma and alveolus provides support for the concept that soluble mediators/ chemoattractants preferentially compartmentalized in the airspaces could promote chemotaxis.

Mechanistically, in addition to increased local effector cells, the enhanced inflammation and tissue damage seen in the lungs of mice with IRD appear to be mediated in part by reactive oxygen/ nitrogen species. In previous work in a CD4-depleted model, we demonstrated elevations in the level of total NO production and inducible NO synthase (iNOS) protein expression in the BALF cell pellet during PCP (50, 60). In this study, the BALF from IRD, *Pneumocystis*-infected mice contained increased levels of both total NO and nitrite. We have previously shown both in PCP and in bleomycin-induced lung injury that enhanced NO/ nitrite correlate with levels of 3-nitrotyrosine, a marker of oxidative-nitrative stress arising from the reactive product of NO and superoxide (50, 53, 61). Taken together, the data are consistent with the concept that despite clearance of the organism, NO and its metabolites produced locally rapidly interact with molecular targets in the lung to promote damage. The present data also raise the possibility of using selective inhibition of iNOS as a therapeutic strategy to limit lung damage from NO-mediated inflammation that occurs during IRD. A

similar approach of iNOS modulation has been shown to be effective in limiting damage in bleomycin models of injury (62).

In addition to direct tissue damage by reactive oxygen/nitrogen species, posttranslational modification of selected protein targets by NO could also occur. One such target of NO appears to be SP-D. It is well known that the lung collectins can modulate both pro- and antiinflammatory effects in vitro and in vivo (50, 53, 63–69). Recently, mechanistic insights into this conundrum have been reported. Using SP-A as the model, the immunomodulatory effects of lung collectins on macrophage function can be attributed in part to selective engagement of two different cell surface receptors capable of interacting with distinct spatial domains in the carbohydrate recognition head domain and N-terminal tail region present in SP-A and SP-D (70).

We have recently extended this concept by demonstrating that the dichotomous functional nature of SP-D can be attributed to alterations in its multimeric structure by NO (25). In its native multimeric form, SP-D is antiinflammatory, down-regulating the inflammatory responses of effector cells. However, in vitro, the transnitrosylation of SP-D with *S*-nitrosocysteine produces *S*-nitrosylation of two key cysteine residues (Cys^{15}/Cys^{20}), resulting in disruption of normal quaternary structure (dodecamer) to produce predominantly monomeric and trimeric SNO-SPD that is chemoattractive for RAW macrophages and induces p38 MAPK phosphorylation mediated by binding to calreticulin/CD91. This observation led us to hypothesize that *S*-nitrosylation of SP-D was the molecular basis for the enhanced lung injury seen in IRD associated with PCP. Multiple findings documented in the present work support this concept. First, the increase in lung inflammation observed in IRD mice was accompanied by increases in alveolar levels of SP-D. In previous models of *P. murina* infection, increases in SP-D occurred late in the course of pulmonary infection (8, 71). During IRD, *P. murina*-infected mice subjected to withdrawal of GK1.5 had even greater increases in total SP-D protein, but there was an associated marked alteration in its higher order structure. Second, *S*-nitrosylation of SP-D was observed in IRD. Third, faster migrating forms of SP-D were seen in native gel electrophoresis corresponding to these monomeric and trimeric forms (25) and were exclusively and markedly enhanced by immunoreconstitution and not *P. murina* infection alone (Fig. 9). Fourth, treatment of BALF with ascorbic acid, which, based on its redox potential, selectively reduces *S*-nitrosylated proteins to release NO (52), blocked the chemotactic activity of BALF obtained from IRD mice (Fig. 10).

The modification of SP-D by inflammation during IRD represents an important emerging paradigm in local immunoregulation in the lung and extends previous similar biochemical and functional observations in a noninfectious mouse model of lung injury. In two previous studies, we have shown that administration of bleomycin to mice produces large amounts of macrophage-driven pulmonary inflammation that was also associated with formation of *S*-nitrosylated SP-D (25, 53). Furthermore, treatment with either anti-SP-D or ascorbic acid blocks macrophage chemotaxis in vitro (25). Similarly, treatment of IRD BALF with ascorbate in the present study also blocked chemotaxis. The effect of ascorbate on macrophage chemotaxis is unlikely to be due to direct effects of ascorbate on macrophages. We have shown that ascorbic acid is impermeable to many biological membranes (72), so

significant alterations in intracellular concentrations are not likely. Additionally, the control BALF (6 wk of PCP) in Fig. 10*B* was also treated with ascorbate and there was no effect on baseline chemotaxis. Therefore, it seems unlikely that there is either a significant effect on macrophages directly (apart from that of SNO-SP-D) or a modification of other components of the BALF by ascorbate treatment sufficient to alter chemotaxis. Finally, we have previously shown that in vitro *S*-nitrosylation of BALF from SP-D knockout mice using the SNO donor *S*-nitrosocysteine has no effect on p38 phosphorylation in RAW macrophages, indicating that NO produced during inflammation is exclusively targeting SP-D and not other protein components (e.g., SP-A, albumin) of BALF. Taken together, although chemokines such as MCP-1 are elevated during PCP and IRD (Ref. 73 and this study), the chemotactic activity of BALF from IRD mice is almost exclusively attributable to SNO-SP-D.

In conclusion, IRD in a mouse model using withdrawal of GK1.5 is associated with enhanced pulmonary injury and proinflammatory events. In parallel, IRD-mediated lung injury was associated with marked increases in BALF levels of SP-D. In vitro, the BALF showed enhanced nitrosylation of SP-D and promoted increased chemotaxis in a macrophage cell line in vitro. Thus, inflammation during IRD represents a feed-forward system in which the additional inflammation leads to further modification of SP-D by NO and subsequent proinflammatory effects mediated by these smaller SP-D forms. This study thus emphasizes the delicate balance that exists between collectins, the innate immune system, and pulmonary inflammation. Therapeutically, it is possible that the balance between modified and unmodified SP-D could modulate the relative degree of inflammation observed in lung injury, leading to the potential therapeutic use of native, multimeric SP-D-containing surfactants. Furthermore, as an alternative strategy, the local inhibition of NO production may in fact lead to decreased posttranslational modification of SP-D and limit the feed-forward inflammatory response and lung damage.

Acknowledgments

We thank Helchem Kadire for expert technical assistance in the generation and maintenance of the murine models used in these studies.

References

1. Stansell JD, Osmond DH, Charlebois E, LaVange L, Wallace JM, Alexander BV, Glassroth J, Kvale PA, Rosen MJ, Reichman LB, et al. Predictors of *Pneumocystis carinii* pneumonia in HIV-infected persons: Pulmonary Complications of HIV Infection Study Group. Am J Respir Crit Care Med. 1997; 155:60–66. [PubMed: 9001290]
2. Su TH, Martin WJ 2nd. Pathogenesis and host response in *Pneumocystis carinii* pneumonia. Annu Rev Med. 1994; 45:261–272. [PubMed: 8198382]
3. Kovacs JA, Hiemenz JW, Macher AM, Stover D, Murray HW, Shelhamer J, Lane HC, Urmacher C, Honig C, Longo DL. *Pneumocystis carinii* pneumonia: a comparison between patients with the acquired immunodeficiency syndrome and patients with other immunodeficiencies. Ann Intern Med. 1984; 100:663–671. [PubMed: 6231873]
4. Huang L, Morris A, Limper AH, Beck JM. and on behalf of the ATS Pneumocystis Workshop Participants. An Official ATS Workshop Summary: recent advances and future directions in *Pneumocystis* pneumonia (PCP). Proc Am Thorac Soc. 2006; 3:655–664. [PubMed: 17065370]

5. Kovacs JA V, Gill J, Meshnick S, Masur H. New insights into transmission, diagnosis, and drug treatment of *Pneumocystis carinii* pneumonia. J Am Med Assoc. 2001; 286:2450–2460.
6. Beers MF, Atochina EN, Preston AM, Beck JM. Inhibition of lung surfactant protein B expression during *Pneumocystis carinii* pneumonia in mice. J Lab Clin Med. 1999; 133:423–433. [PubMed: 10235125]
7. Atochina EN, Beers MF, Scanlon ST, Preston AM, Beck JM. *P. carinii* induces selective alterations in component expression and biophysical activity of lung surfactant. Am J Physiol. 2000; 278:L599–L609.
8. Atochina EN, Beck JM, Scanlon ST, Preston AM, Beers MF. *Pneumocystis carinii* pneumonia alters expression and distribution of lung collectins SP-A and SP-D. J Lab Clin Med. 2001; 137:429–439. [PubMed: 11385364]
9. Wright TW, Notter RH, Wang ZD, Harmsen AG, Gigliotti F. Pulmonary inflammation disrupts surfactant function during *Pneumocystis carinii* pneumonia. Infect Immun. 2001; 69:758–764. [PubMed: 11159965]
10. Wiedmann HP. Surfactant and acquired lung diseases. J Lab Clin Med. 1996; 127:239–241. [PubMed: 9273354]
11. Martin WJ, Wright JR. *Pneumocystis carinii* pneumonia and pulmonary surfactant. J Lab Clin Med. 1999; 133:406–407. [PubMed: 10235122]
12. Griese M. Pulmonary surfactant in health and human lung diseases: state of the art. Eur Respir J. 1999; 13:1455–1476. [PubMed: 10445627]
13. Rooney SA, Young SL, Mendelson CR. Molecular and cellular processing of lung surfactant. FASEB J. 1994; 8:957–967. [PubMed: 8088461]
14. Crouch EC. Collectins and pulmonary host defense. Am J Respir Cell Mol Biol. 1998; 19:177–201. [PubMed: 9698590]
15. Possmayer F. A proposed nomenclature for pulmonary surfactant-associated proteins. Am Rev Respir Dis. 1988; 138:990–998. [PubMed: 3059887]
16. Curstedt T, Jornvall H, Robertson B, Bergman T, Berggren P. Two hydrophobic low-molecular-mass protein fractions of pulmonary surfactant: characterization and biophysical activity. Eur J Biochem. 1987; 168:255–262. [PubMed: 3665923]
17. Weaver TE, Na CL, Stahlman M. Biogenesis of lamellar bodies, lysosome-related organelles involved in storage and secretion of pulmonary surfactant. Semin Cell Dev Biol. 2002; 13:263–270. [PubMed: 12243725]
18. Crouch EC, Wright JR. Surfactant proteins A and D and pulmonary host defense. Annu Rev Physiol. 2001; 63:521–554. [PubMed: 11181966]
19. Crouch E, Hartshorn K, Ofek I. Collectins and pulmonary innate immunity. Immunol Rev. 2000; 173:52–65. [PubMed: 10719667]
20. Wright JR. Immunoregulatory functions of surfactant proteins. Nat Rev Immunol. 2005; 5:58–68. [PubMed: 15630429]
21. Crouch E, Persson A, Chang D, Heuser J. Molecular structure of pulmonary surfactant protein D (SP-D). J Biol Chem. 1994; 269:17311–17319. [PubMed: 8006040]
22. Crouch E, Parghi D, Kuan SF, Persson A. Surfactant protein D: subcellular localization in nonciliated bronchiolar epithelial cells. Am J Physiol. 1992; 263:L60–L66. [PubMed: 1636730]
23. Zhang PN, McAlinden A, Li S, Schumacher T, Wang HL, Hu SS, Sandell L, Crouch E. The amino-terminal heptad repeats of the coiled-coil neck domain of pulmonary surfactant protein D are necessary for the assembly of trimeric subunits and dodecamers. J Biol Chem. 2001; 276:19862–19870. [PubMed: 11279100]
24. Brown-Augsburger P, Chang D, Rust K, Crouch EC. Biosynthesis of surfactant protein D: contributions of conserved NH_2-terminal cysteine residues and collagen helix formation to assembly and secretion. J Biol Chem. 1996; 271:18912–18919. [PubMed: 8756121]
25. Guo CJ, Atochina-Vasserman EN, Abramova E, Foley JP, Zaman A, Crouch E, Beers MF, Savani RC, Gow AJ. *S*-nitrosylation of surfactant protein-D controls inflammatory function. PLoS Biol. 2008; 6:e266. [PubMed: 19007302]

26. Barry SM, Lipman MCI, Deery AR, Johnson MA, Janossy G. Immune reconstitution pneumonitis following *Pneumocystis carinii* pneumonia in HIV-infected subjects. HIV Med. 2002; 3:207–211. [PubMed: 12139660]
27. Koval CE, Gigliotti F, Nevins D, Demeter LM. Immune reconstitution syndrome after successful treatment of *Pneumocystis carinii* pneumonia in a man with human immunodeficiency virus type 1 infection. Clin Infect Dis. 2002; 35:491–493. [PubMed: 12145736]
28. Wislez M, Bergot E, Antoine M, Parrot A, Carette MF, Mayaud C, Cadranel J. Acute respiratory failure following HAART introduction in patients treated for *Pneumocystis carinii* pneumonia. Am J Respir Crit Care Med. 2001; 164:847–851. [PubMed: 11549544]
29. Wu AKL V, Cheng CC, Tang BSF, Hung IFN, Lee RA, Hui DS, Yuen KY. The unmasking of *Pneumocystis jiroveci* pneumonia during reversal of immunosuppression: case reports and literature review. BMC Infect Dis. 2004; 4:57. [PubMed: 15588295]
30. Cheng VCC I, Hung FN, Wu AKL, Tang BSF, Chu CM, Yuen KY. Lymphocyte surge as a marker for immunorestitution disease due to *Pneumocystis jiroveci* pneumonia in HIV-negative immunosuppressed hosts. Eur J Clin Microbiol Infect Dis. 2004; 23:512–514. [PubMed: 15141339]
31. Beck JM, Rosen MJ, Peavy HH. Pulmonary complications of HIV infection: Report of the Fourth NHLBI Workshop. Am J Respir Crit Care Med. 2001; 164:2120–2126. [PubMed: 11739145]
32. Wright TW, Johnston CJ, Harmsen AG, Finkelstein JN. Chemokine gene expression during *Pneumocystis carinii* driven pulmonary inflammation. Infect Immun. 1999; 67:3452–3460. [PubMed: 10377126]
33. Wright TW, Gigliotti F, Finkelstein JN, McBride JT, An CL, Harmsen AG. Immune-mediated inflammation directly impairs pulmonary function, contributing to the pathogenesis of *Pneumocystis carinii* pneumonia. J Clin Invest. 1999; 104:1307–1317. [PubMed: 10545529]
34. Bhagwat SP, Gigliotti F, Xu HD, Wright TW. Contribution of T cell subsets to the pathophysiology of *Pneumocystis*-related immunorestitution disease. Am J Physiol. 2006; 291:L1256–L1266.
35. Chen WX, Mills JW, Harmsen AG. Development and resolution of *Pneumocystis-carinii* pneumonia in severe combined immunodeficient mice: morphological study of host inflammatory responses. Int J Exp Pathol. 1992; 73:709–720. [PubMed: 1493101]
36. Roths JB, Sidman CL. Both immunity and hyperresponsiveness to *Pneumocystis carinii* result from transfer of $CD4^+$ but not $CD8^+$ T-cells into severe combined immunodeficiency mice. J Clin Invest. 1992; 90:673–678. [PubMed: 1353767]
37. Shellito JE V, Suzara V, Blumenfeld W, Beck JM, Steger HJ, Ermak TH. A new model of *Pneumocystis carinii* infection in mice selectivity depleted of helper T lymphocytes. J Clin Invest. 1990; 85:1686–1693. [PubMed: 2139668]
38. Beck JM, Harmsen AG. Lymphocytes in host defense against*Pneumocystis carinii*. Semin Respir Infect. 1998; 13:330–338. [PubMed: 9872630]
39. Harmsen AG, Stankiewicz M. Requirement for $CD4^+$ cells in resistance to *Pneumocystis carinii* pneumonia in mice. J Exp Med. 1990; 172:937–945. [PubMed: 2117637]
40. Beers MF, Bates SR, Fisher AB. Differential extraction for the rapid purification of bovine surfactant protein B. Am J Physiol. 1992; 262:L773–L778. [PubMed: 1616060]
41. Beers MF, Wali A, Eckenhoff MF, Feinstein SI, Fisher JH, Fisher AB. An antibody with specificity for surfactant protein C precursors: identification of pro-SP-C in rat lung. Am J Respir Cell Mol Biol. 1992; 7:368–378. [PubMed: 1389209]
42. Beck JM, Newbury RL, Palmer BE, Warnock ML, Byrd PK, Kaltrieder HB. Role of $CD8^+$ lymphocytes in host defense against *Pneumocystis carinii* in mice. J Lab Clin Med. 1996; 128:477–487. [PubMed: 8900290]
43. Beck JM, Liggit HD, Brunette EN, Fuchs HJ, Shellito JE, Debs RJ. Reduction in intensity of *Pneumocystis carinii* pneumonia in mice by aerosol administration of gamma interferon. Infect Immun. 1991; 59:3859–3862. [PubMed: 1682252]
44. Rudmann DG, Preston AM, Moore MW, Beck JM. Susceptibility to *Pneumocystis carinii* in mice is dependent on simultaneous deletion of IFN-γ and type 1 and 2 TNF receptor genes. J Immunol. 1998; 161:360–366. [PubMed: 9647244]

45. Zheng MQ, Shellito JE, Marrero L, Zhong Q, Julian S, Ye P, Wallace V, Schwarzenberger P, Kolls JK. $CD4^+$ T cell-independent vaccination against *Pneumocystis carinii* in mice. J Clin Invest. 2001; 108:1469–1474. [PubMed: 11714738]
46. Phares TW, Kean RB, Mikheeva T, Hooper DC. Regional differences in blood-brain barrier permeability changes and inflammation in the apathogenic clearance of virus from the central nervous system. J Immunol. 2006; 176:7666–7675. [PubMed: 16751414]
47. Jassar AS, Suzuki E, Kapoor V, Sun J, Silverberg MB, Cheung LM, Burdick MD, Strieter RM, Ching LM, Kaiser LR, Albelda SM. Activation of tumor-associated macrophages by the vascular disrupting agent 5,6-dimethylxanthenone-4-acetic acid induces an effective $CD8^+$T-cell-mediated antitumor immune response in murine models of lung cancer and mesothelioma. Cancer Res. 2005; 65:11752–11761. [PubMed: 16357188]
48. Bradford MM. A rapid and sensitive method for the quantitation of microgram quantities of protein utilizing the principle of protein-dye binding. Ann Biochem. 1976; 72:248–254.
49. Bartlett GR. Phosphorous assay in column chromatography. J Biol Chem. 1959; 234:466–468. [PubMed: 13641241]
50. Atochina EN, Gow AJ, Beck JM, Haczku A, Inch A, Kadire H, Tomer Y, Davis C, Preston AM, Poulain F, et al. Surfactant protein D deficient mice exhibit delayed clearance of *Pneumocystis* lung infection with increased inflammation and altered nitric oxide metabolism. J Infect Dis. 2004; 189:1528–1539. [PubMed: 15073692]
51. Enhorning G. Pulmonary surfactant function studied with the pulsating bubble surfactometer (PBS) and the capillary surfactometer (CS). Comp Biochem Physiol A Mol Integr Physiol. 2001; 129:221–226. [PubMed: 11369546]
52. Jaffrey SR, Snyder SH. The biotin switch method for the detection of *S*-nitrosylated proteins. Sci STKE. 2001; 2001:pl1. [PubMed: 11752655]
53. Casey J, Kaplan J, Atochina-Vasserman EN, Gow AJ, Kadire H, Tomer Y, Fisher JH, Hawgood S, Savani RC, Beers MF. Alveolar surfactant protein D content modulates bleomycin-induced lung injury. Am J Respir Crit Care Med. 2005; 172:869–877. [PubMed: 15994463]
54. Fang KZ, Ragsdale NV, Carey RM, Macdonald T, Gaston B. Reductive assays for *S*-nitrosothiols: implications for measurements in biological systems. Biochem Biophys Res Commun. 1998; 252:535–540. [PubMed: 9837741]
55. Meissner NN, Swain S, Tighe M, Harmsen A, Harmsen A. Role of type I IFNs in pulmonary complications of *Pneumocystis murina* infection. J Immunol. 2005; 174:5462–5471. [PubMed: 15843544]
56. Shellito JE, Tate C, Ruan S, Kolls J. Murine $CD4^+$ T lymphocyte subsets and host defense against*Pneumocystis carinii*. J Infect Dis. 2000; 181:2011–2017. [PubMed: 10837183]
57. Pottratz S, Weir AL. Attachment of *Pneumocystis carinii* to primary cultures of rat alveolar epithelial cells. Exp Cell Res. 1995; 221:357–362. [PubMed: 7493634]
58. Beck JM, Preston AM, Wagner JG, Wilcoxen SE, Hossler P, Meshnick SR, Paine R. Interaction of rat *Pneumocystis carinii* and rat alveolar epithelial cells in vitro. Am J Physiol. 1998; 19:L118–L125. [PubMed: 9688943]
59. Garvy BA, Wiley JA, Gigliotti F, Harmsen AG. Protection against *Pneumocystis carinii* pneumonia by antibodies generated from either T helper 1 or T helper 2 responses. Infect Immun. 1997; 65:5052–5056. [PubMed: 9393795]
60. Shellito JE, Kolls JK, Olariu R, Beck JM. Nitric oxide and host defense against *Pneumocystis carinii* infection in a mouse model. J Infect Dis. 1996; 173:432–439. [PubMed: 8568306]
61. Ischiropoulos H, Beers MF, Ohnishi ST, Fisher D, Garner S, Thom SR. Nitric oxide production and perivascular tyrosine nitration in brain following carbon monoxide poisoning in the rat. J Clin Invest. 1996; 97:2260–2267. [PubMed: 8636405]
62. Genovese T, Cuzzocrea S, Di Paola R, Failla M, Mazzon E, Sortino M, Frasca G, Gili E, Crimi N, Caputi A, Vancheri C. Inhibition or knock out of inducible nitric oxide synthase result in resistance to bleomycin-induced lung injury. Respir Res. 2005; 6:58. [PubMed: 15955252]
63. Borron P, Veldhuizen RA, Lewis JF, Possmayer F, Caveney A, Inchley K, McFadden RG, Fraher LJ. Surfactant associated protein-A inhibits human lymphocyte proliferation and IL-2 production. Am J Respir Cell Mol Biol. 1996; 15:115–121. [PubMed: 8679215]

64. Borron P, McIntosh JC, Korfhagen TR, Whitsett JA, Taylor J, Wright JR. Surfactant-associated protein A inhibits LPS-induced cytokine and nitric oxide production in vivo. Am J Physiol. 2000; 278:L840–L847.

65. Koptides M, Umstead TM, Floros J, Phelps DS. Surfactant protein A activates NF-kappa B in the THP-1 monocytic cell line. Am J Physiol. 1997; 17:L382–L388. [PubMed: 9277450]

66. Atochina EN, Beers MF, Hawgood S, Poulain F, Davis C, Fusaro TT, Gow AJ. Surfactant protein-D, a mediator of innate lung immunity, alters the products of nitric oxide metabolism. Am J Respir Cell Mol Biol. 2003; 30:271–279. [PubMed: 12871850]

67. Atochina EN, Beck JM, Preston AM, Haczku A, Tomer Y, Scanlon ST, Fusaro T, Casey J, Hawgood S, Gow AJ, Beers MF. Enhanced lung injury and delayed clearance of *Pneumocystis carinii* in surfactant protein A-deficient mice: attenuation of cytokine responses and reactive oxygen-nitrogen species. Infect Immun. 2004; 72:6002–6011. [PubMed: 15385504]

68. Hawgood S, Brown C, Edmondson J, Stumbaugh A, Allen L, Goerke J, Clark H, Poulain F. Pulmonary collectins modulate strain-specific influenza A virus infection and host responses. J Virol. 2004; 78:8565–8572. [PubMed: 15280465]

69. Clark H, Palaniyar N, Strong P, Edmondson J, Hawgood S, Reid KBM. Surfactant protein D reduces alveolar macrophage apoptosis in vivo. J Immunol. 2002; 169:2892–2899. [PubMed: 12218102]

70. Gardai SJ, Xiao YQ, Dickinson M, Nick JA, Voelker DR, Greene KE, Henson PM. By binding SIRPα or calreticulin/CD91, lung collectins act as dual function surveillance molecules to suppress or enhance inflammation. Cell. 2003; 115:13–23. [PubMed: 14531999]

71. Limper AH, O'Riordan DM, Vuk-Pavlovic Z, Crouch EC. Accumulation of surfactant protein D in the lung during *Pneumocystis carinii* pneumonia. J Eukaryot Microbiol. 1994; 41:98S. [PubMed: 7804292]

72. Beers MF, Johnson RG, Scarpa A. Evidence for an ascorbate shuttle for the transfer of reducing equivalents across chromaffin granule membranes. J Biol Chem. 1986; 261:2529–2535. [PubMed: 3949732]

73. Wang J, Gigliotti F, Bhagwat SP, Maggirwar SB, Wright TW. *Pneumocystis* stimulates MCP-1 production by alveolar epithelial cells through a JNK-dependent mechanism. Am J Physiol. 2007; 292:L1495–L1505.

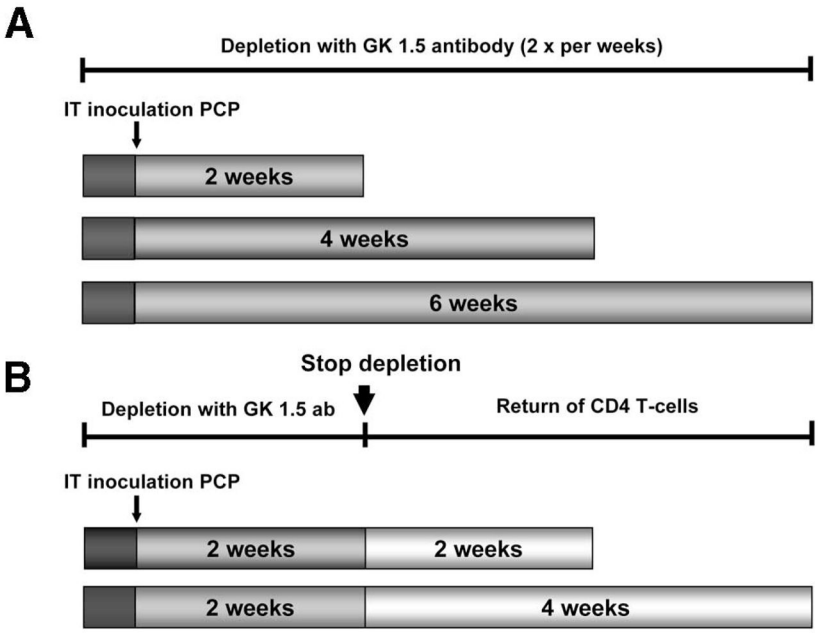

FIGURE 1.

CD4-depleted mouse model of PCP and IRD. *A*, C57BL/6 mice were immunosuppressed by selective CD4 depletion via i.p. injection twice weekly with the mAb GK1.5. One week following the initiation of CD4 depletion, mice were inoculated with *P. murina* cysts as described in *Materials and Methods.* Immunosuppression was continued for 2, 4, and 6 wk to promote *P. murina* infection as previously published (42). *B*, IRD was produced by discontinuation of immunosuppression through withdrawal of GK1.5 2 wk after inoculation. Mice were then sacrificed 2 or 4 wk (i.e. 2 wk + 2 wk or 2 wk + 4 wk groups, respectively) after removal of GK1.5.

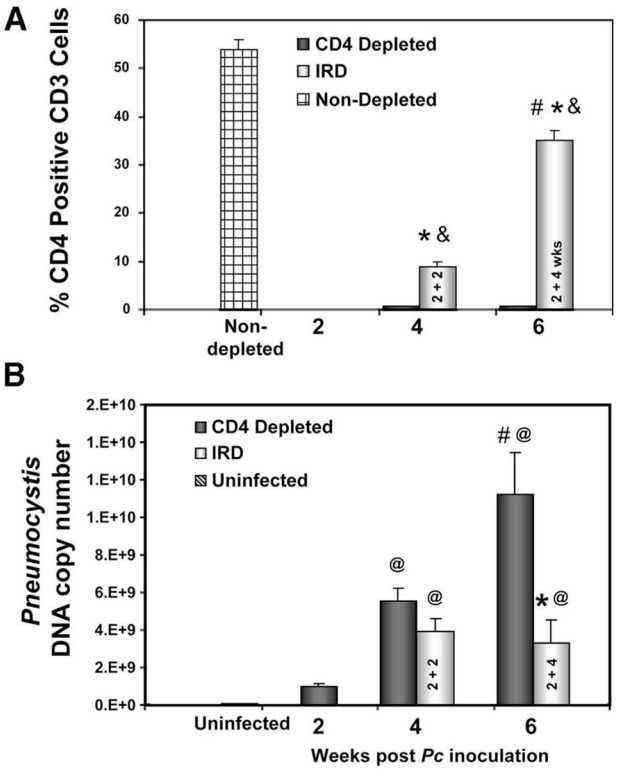

FIGURE 2.

Recovery of $CD4^+$ cells after withdrawal of GK1.5 Ab results in clearance of *P. murina*. PCP in continuously CD4-depleted mice and IRD mice were generated as described in *Materials and Methods* and schematically illustrated in Fig. 1. A, For flow cytometric analysis, total spleen cells stained for CD3 and CD4 as described in *Materials and Methods* were subjected to FACS. The data were expressed as the percentage of CD4 expressing $CD3^+$ T cells (mean ± SEM; $n = 4–8$ in each group). At baseline, nondepleted controls demonstrated 54% $CD4^+$ T cells. *, $p < 0.05$ for reconstituted group vs corresponding CD4-depleted group at the same interval postinfection; #, $p < 0.05$ vs from corresponding treatment group; &, $p < 0.05$ vs nondepleted mice. *B*, *P. murina* burden after withdrawal of GK1.5. Viable *P. murina* were quantitated by real-time PCR measurement of rRNA copy number using a standard curve of known copy number of *P. murina* 18S RNA as described in *Materials and Methods*. Data are expressed logarithmically as copy number (mean ± SEM; $n = 4–8$ in each group). *, $p < 0.05$ for IRD mice vs corresponding CD4-depleted group at same time post infection; #, $p < 0.05$ vs from corresponding treatment group; @, $p < 0.05$ vs CD4-depleted PCP group 2 wk postinoculation.

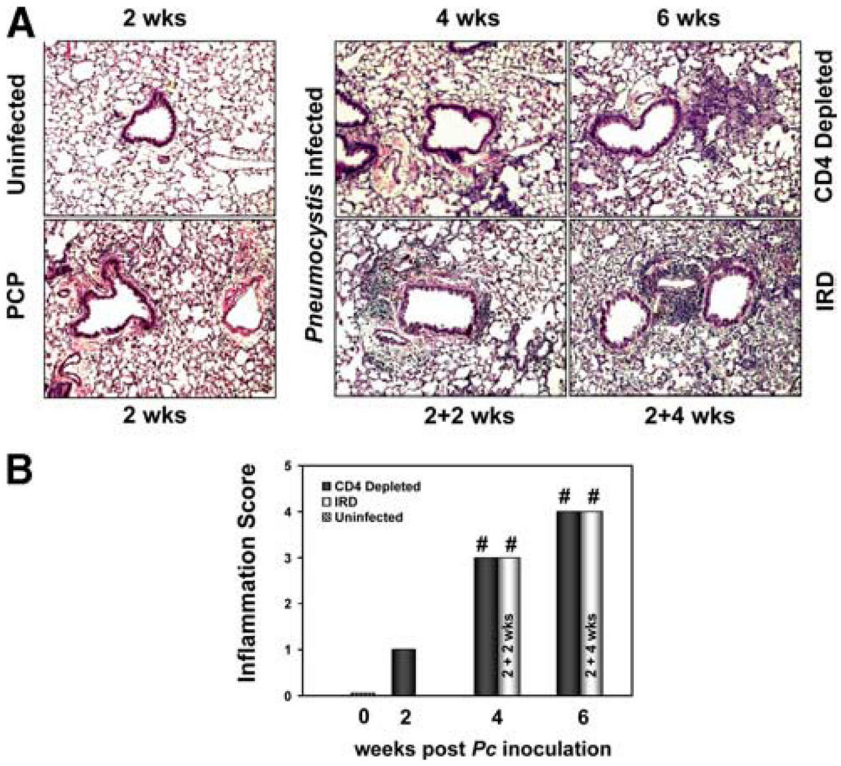

FIGURE 3.

Immune reconstitution following *P. murina* infection induces significant worsening of lung inflammation. *A*, Representative morphological changes in formalin-fixed, paraffin-embedded, H&E-stained right lung sections prepared from uninfected and *P. murina*-infected CD4-depleted or IRD mice harvested 2, 4, and 6 wk postinoculation as labeled. Original magnification ×100. *B*, Histological scoring of lung inflammation. Median inflammation scores were determined by blinded evaluation of stained sections from each treatment group as described in *Materials and Methods*. #, $p < 0.05$ vs CD4-depleted 2 wk *P. murina* infected group.

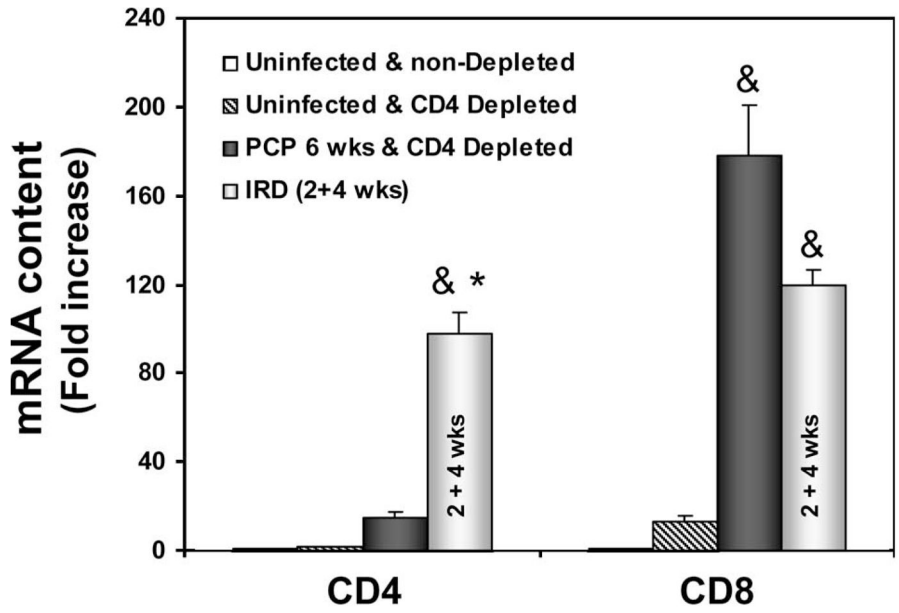

FIGURE 4.

Immune reconstitution following *P. murina* infection induces infiltration of lung parenchyma by CD4 and CD8 cells. Total RNA isolated from the left lungs of mice as in Fig. 2 was reverse transcribed, and CD4, CD8, and 18S RNA signals were amplified as described in *Materials and Methods.* Ct values obtained were normalized to 18S signals and further analyzed using the relative quantitation (ΔΔCt) method. Data are expressed as fold change (mean ± SEM; $n = 5$ in each group). *, $p < 0.05$ for IRD mice vs corresponding CD4-depleted group at same time postinfection; &, $p < 0.05$ vs uninfected and nondepleted group.

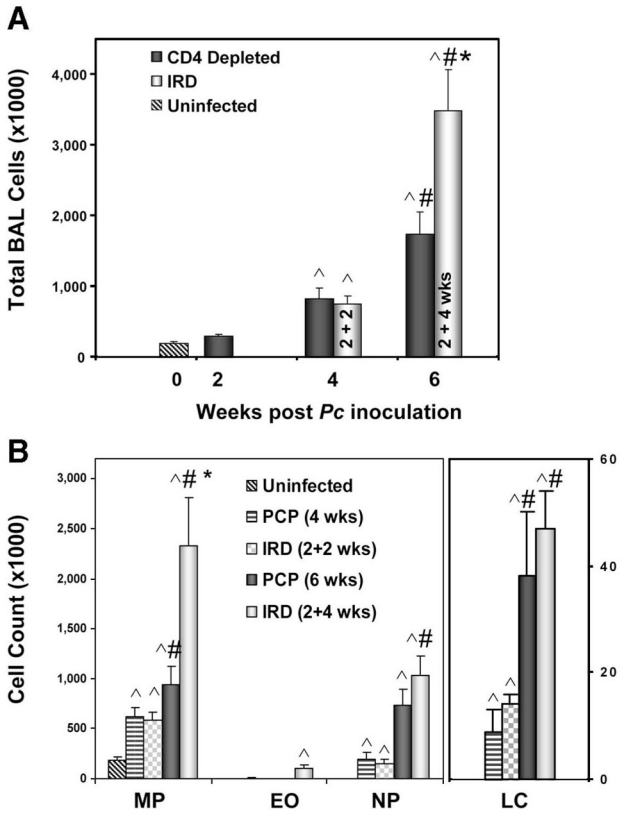

FIGURE 5.

P. murina in immune-reconstituted mice is associated with increased BALF cellularity. *A*, Total BALF cell counts and (*B*) differential cell counts for macrophages (MP), lymphocytes (LC), eosinophils (EO), and neutrophils (NP) were performed as described in *Materials and Methods* in *P. murina*-infected CD4-depleted or IRD mice harvested 2, 4, and 6 wk postinoculation. The data are expressed as cell numbers × 1000. Values are shown as mean ± SEM (n = 5–20 animals in each group). Multiple comparisons were made by ANOVA. *, $p < 0.05$ for IRD mice vs corresponding CD4-depleted group at same time postinfection; #, $p < 0.05$ vs corresponding treatment group; ^, $p < 0.05$ vs uninfected group.

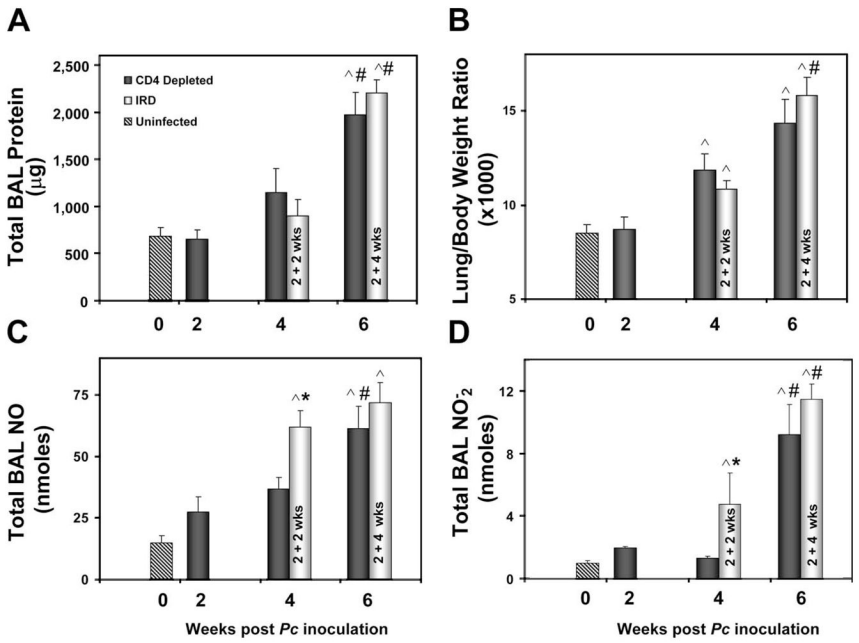

FIGURE 6.

Lung injury by *P. murina* infection is enhanced in IRD mice. *A*, Total protein content of BALF fractions of uninfected and *P. murina*-infected CD4-depleted or IRD mice was determined as described in *Materials and Methods*. Data are expressed as mean ± SEM (μg) per mouse. *B*, Body weights and lung weights from uninfected and *P. murina*-infected CD4-depleted or IRD mice were recorded. Group mean data (±SEM) are expressed as a ratio of lung-to-body weight at terminal endpoints. *C* and *D*, Quantitation of total NO (*C*) and nitrates (*D*) in BALF of uninfected and *P. murina*-infected CD4-depleted or IRD mice. BALF samples were analyzed by chemical reduction and chemiluminesence as described in *Materials and Methods*. Data are expressed as mean ± SEM (in nmol); $n = 4–8$ in each group. For all panels, *, $p < 0.05$ for IRD mice vs corresponding CD4-depleted group at same time postinfection; #, $p < 0.05$ vs corresponding treatment group; ^, $p < 0.05$ vs uninfected group.

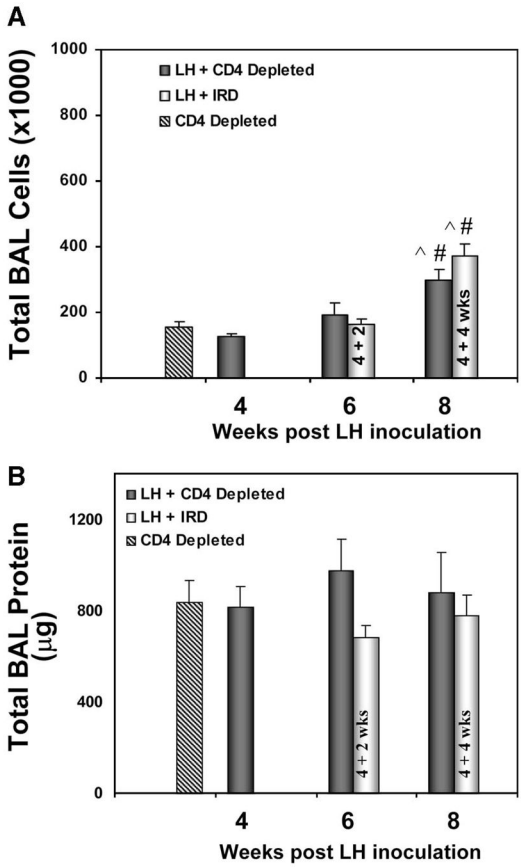

FIGURE 7.

Immunoreconstitution of C57BL/6 mice following inoculation with allogenenic lung homogenate does not produce significant lung injury. CD4-depleted C57BL/6 mice were inoculated with 100 *μ*l of lung homogenate (LH) from uninfected *nu*/*nu* (BALB/c background) donors. A control group consisted of mice subjected to CD4 depletion only for 6 wk (CD4 Depleted). Four weeks postinoculation, GK1.5 was withheld from indicated groups (4 + 2; 4 + 4) to produce immunoreconstitution. Mice were sacrificed as indicated at 4, 6, and 8 wk after LH inoculation. *A*, Total BALF cell counts were determined using a Coulter counter as described in *Materials and Methods*. Data are expressed as cell numbers × 1000. Values are shown as mean ± SEM (*n* × 5–7 animals in each group). *B*, Total protein content of BALF fractions was determined by the method of Bradford (48). Data are expressed as mean ± SEM (*μ*g) per mouse.

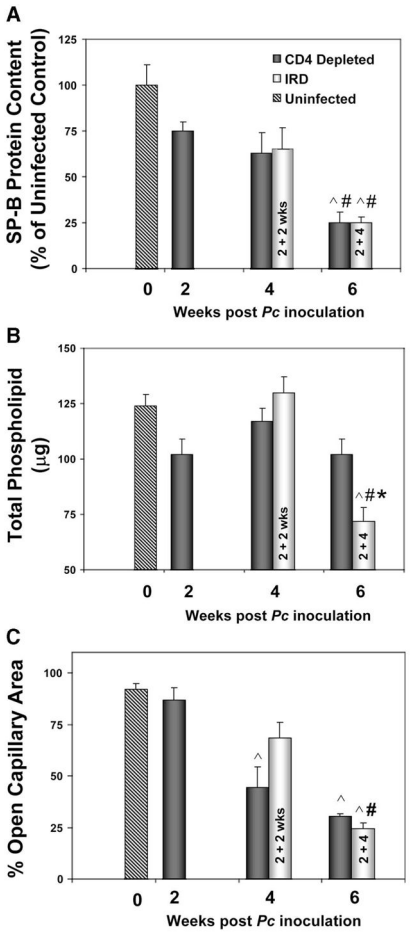

FIGURE 8.

Surfactant biophysics and function are impaired in IRD mice. At the indicated time postinoculation, the biophysically active LA surfactant fraction was prepared from harvested BALF. *A*, Samples of LA fractions were separated by SDS-PAGE and immunoblotted with SP-B Ab as described in *Materials and Methods*. Band density was quantified and is expressed as percentage of uninfected level (mean ± SEM; $n = 5$ in each group). *B*, Total phospholipid in LA was estimated using a modification of the colorimetric Bartlett method as described in *Materials and Methods*. Data are expressed as mean ± SEM (μg) of n =10–20 samples. *C*, Surface activity of LA surfactant was determined by measuring capillary openness by capillary surfactometer as described in *Materials and Methods*. Values are obtained by averaging triplicate measurements of each sample and group mean data (mean ± SEM, expressed as percentage of capillary openness (100 being fully open); $n = 4$–6 samples/time point). For all panels, * $p < 0.05$ for IRD mice vs corresponding CD4-depleted group at same time postinfection; #, $p < 0.05$ vs corresponding treatment group; ^, $p < 0.05$ vs uninfected group.

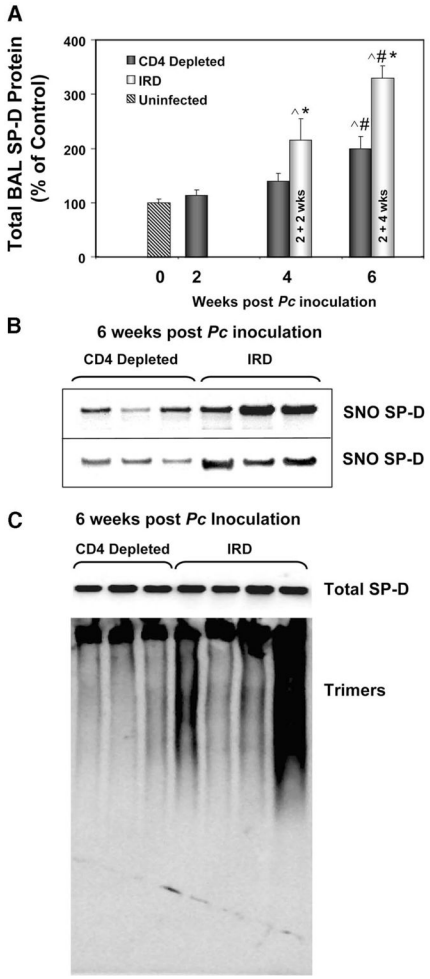

FIGURE 9.

IRD alters the quaternary structure of SP-D and production of SNO-SP-D. *A*, Total SP-D in BALF was determined by Western blotting and densitometric scanning as described in *Materials and Methods*. Data were normalized to uninfected control and are reported as mean ± SEM (expressed as percentage of control; $n = 4–6$ samples per time point). *, $p < 0.05$ for IRD mice vs corresponding CD4-depleted group at same time postinfection; #, $p < 0.05$ vs corresponding treatment group; ^, $p < 0.05$ vs uninfected group. *B*, BALF from *P. murina*-infected CD4-depleted or IRD mice 6 wk postinoculation was analyzed for SNO-SP-D content by the biotin switch assay as described in *Materials and Methods*. Shown are blots obtained from two separate analyses of two independent experiments. SNO-SP-D formation is consistently increased in the IRD samples. *C*, BALF normalized for equal calculated amounts of total SP-D (as determined by reduced SDS PAGE) in *A* from *P. murina*-infected CD4-depleted or IRD mice 6 wk postinoculation was analyzed by native PAGE and Western blotting with SP-D antiserum to determine quaternary structure of SP-D. Multimeric SP-D is incapable of entering the gel at the top, while smaller molecular mass forms are seen only in BALF from reconstituted mice. Data are representative of duplicate determinations from two independent experiments.

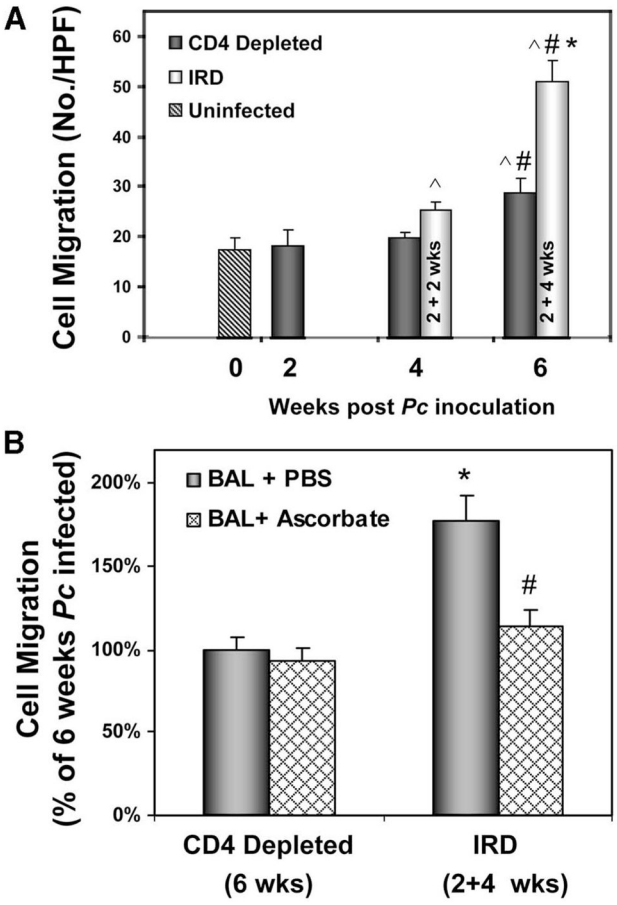

FIGURE 10.

Immune-reconstitution induces macrophage chemotaxis through SNO-SP-D. *A*, BALF from uninfected or *P. murina*-infected CD4-depleted mice with or without IRD was harvested 2, 4, or 6 wk after inoculation and assayed for the ability to induce RAW 264.7 macrophage migration using a modified Boyden chamber. Migration, defined as the number of cells transitioning the barrier membrane after 3 h of incubation, was determined by manual counting. Data represent group mean values (±SEM) from measurements performed in triplicate from two independent experiments and analyzed by ANOVA. *, $p < 0.05$ for IRD mice vs corresponding CD4-depleted group at same time postinoculation; #, $p < 0.05$ vs corresponding treatment group; ^, $p < 0.05$ vs uninfected group. *B*, To eliminate the effect of SNO modification, BALF from *P. murina*-infected CD4-depleted mice or IRD mice was harvested 6 wk after inoculation and pretreated with 20 mM ascorbic acid or PBS as indicated and analyzed for the ability to induce RAW cell chemotaxis in vitro as in *A*. Data are normalized as percentage of *P. murina*-infected continuously CD4-depleted mice (6 wk). All measurements were performed in triplicate and are representative of two independent experiments analyzed by ANOVA. *, $p < 0.05$ for PBS treated BALF from IRD mice vs corresponding CD4-depleted group; #, $p < 0.05$ vs corresponding PBS-treated BAL.

Table I

BALF cytokine levels in Pneumocystis infection and IRD[a]

		Pneumocystis Infected (Weeks Postinoculation)				
		CD4 Depleted			Reconstituted	
Total BALF Cytokine (pg)	**Uninfected (Lung Homogenate): CD4 Depleted**	**2**	**4**	**6**	**2 + 2**	**2 + 4**
INF-γ	72.1 ± 15.4	96.6 ± 21.1	192.1 ± 48.4	231.9 ± 42.1*	220.3 ± 48.3*	256.2 ± 74.7*
TNF-α	10.6 ± 9.0	15.8 ± 7.4	74.2 ± 32.1	143.6 ± 70.9*	97.1 ± 27.3	68.8 ± 35.6
KC	19.2 ± 3.7	37.8 ± 7.4	99.1 ± 22.0	92.3 ± 24.1	149.8 ± 28.9*	169.1 ± 46.3*
Eotaxin	25.0 ± 6.8	27.8 ± 7.7	47.6 ± 7.8	46.3 ± 11.9	54.7 ± 19.0	41.8 ± 9.7
MCP-1	17.1 ± 8.7	20.6 ± 4.3	56.1 ± 11.5	122.2 ± 11.2*	67.2 ± 3.6	192.8 ± 38.1*,#

[a]Multiplex analysis of BALF for all groups for cytokine/chemokine was performed as described in *Materials and Methods.* Data are expressed as total cytokine recovered (in pg) as mean ± SEM (n = 5 in each group). Groups were compared using one-way ANOVA.

*$p < 0.05$ vs uninfected (Lung homogenate inoculated) mice;

#$p < 0.05$ vs 6 wk CD4-depleted *Pneumocystis*-infected group.